文章编号：1001-9014(XXXX)XX-0001-08

DOI:10.11972/j.issn.1001-9014.XXXX.XX.001

Analysis of the effect of vibration on the homogeneity of the kinematic mechanism of an angular mirror translational interferometer

Xu Xue-Rong[1,2], Peng Yi-Tian[1*], Gu Ming-Jian[2*], Jiang Teng-teng[3]

(1. College of Mechanical Engineering, Donghua University, Shanghai 201620, China;
2. Shanghai Institute of Technical Physcics Chinese Academy of Sciences 200083, China;
3. State Key Laboratory of Infrared Physics, Shanghai Institute of Technical Physics, Chinese Academy of Sciences, Shanghai 200083, China)

Abstract: The effect of external vibration on the velocity uniformity of the moving mechanism of the angular mirror translational Fourier transform interferometer (hereinafter referred to as interferometer) can be quantitatively analysed by the interferometer optical range difference velocity stability. The article proposes a more comprehensive method of analysing the optical range difference velocity uniformity for the reliability of the interferometer kinematic mechanism under the influence of on-orbit microvibration in the process of space spectroscopy detection. The method incorporates the structural response of the interferometer caused by external excitation into the stability analysis as one of the influencing factors, so as to reflect the reliability of the interferometer in orbit more realistically, and judge the microvibration criticality that the interferometer can withstand more accurately. At the same time, an optical surface model of the interferometer is established to further theoretically characterise the effect of microvibration on the homogeneity of the interferometric mechanism. The method discussed in the article provides a way of thinking for the judgement of the reliability of the mechanism movement under the external excitation perturbation as well as the research on the optimisation of the mechanism control.

Key words: Fourier-interferometer, optical range difference, velocity stability, tremor, space spectroscopy detection

PACS:

角镜平动式干涉系统在振颤条件下的运动均匀特性研究

徐雪荣[1,2], 彭倚天[1*], 顾明剑[2*], 姜腾腾[3]

(1. 东华大学 机械工程学院,上海 201620;
2. 中国科学院上海技术物理研究所,上海 200083;
3. 中国科学院上海技术物理研究所 红外物理国家重点实验室,上海 200083)

摘要:傅立叶干涉系统(以下简称干涉仪)的光程差速度稳定性指标,可用来对干涉系统运动的速度均匀性进行量化分析。在空间遥感仪器入轨后的振颤环境下,其机构对探测过程中会出现运动可靠性问题,本文针对此工况提出并分析研究了一种新的针对干涉系统光程差的速度均匀性分析方法。外界振颤激励会引起干涉系统结构的响应,该响应可作为干涉系统全新的稳定指标进行分析,可进一步精确定量化干涉系统稳定性性能所受振颤影响,也可表征干涉系统在轨时力学表现。同时,建立干涉仪的光学表面模型,进一步从理论上表征微振动对干涉机理均匀性的影响。该方法对进一步研究外部振颤工况下干涉系统稳定性性能及其控制研究具有一定指导意义。

关 键 词:傅立叶干涉系统;光程差;速度均匀性;振颤;空间遥感

中图分类号:O43　　**文献标识码**:A

Received date: 2024-01-25, **revised date**: 2024-06-25　　**收稿日期**:2024-01-25,**修回日期**:2024-06-25

Biography: Xu Xuerong (1991-), male, Jiangsu Dongtai, master degree candidate. Research area involves Precision optical structure. E-mail: 1028626740@qq.com.

* **Corresponding author**: E-mail: gumingj@sin.com, yitianpeng@dhu.edu.cn.

Introduction

The interferometric Fourier transform spectral detection technology has many advantages such as large detection luminous flux, multiple spectral channels, high spectral resolution, etc. It has gradually become a hot spot for the development of spectral detection technology at home and abroad[1-3]. The purpose of spectral detection is to obtain the spectral information of the measured beam. Spectral detection firstly modulates the measured beam in time or space, and obtains the interference signal of the measured beam; and then carries out Fourier inversion on the interference signal, obtains the spectral information of the measured beam, and completes the task of spectral detection. In the process of spectral detection, the interferometric signal is obtained by the interferometer (in this paper, it refers to the angular mirror translational interferometer), and the interferometric signal directly determines the quality of the spectral map, so the interferometer technology is the key to the spectral detection[4]. In order to obtain high-quality interferometric signals, it is necessary to ensure the precision movement of the linear mechanism of the interferometer itself to achieve the uniform scanning modulation of the interferometric optical range difference. And the high-precision spectral detection puts forward extremely high requirements on the uniformity of the interferometer optical range difference speed. However, after orbiting, the micro-vibration of the flywheel, scanning mechanism, mechanical cooler and other equipments on the satellite will affect the speed uniformity of the interferometer.

Generally speaking, the velocity uniformity of the interferometer is mainly guaranteed by the mechanism control system, but the actual engineering often encounters the situation that the control system's guarantee of uniformity is not clear due to the immaturity of the control algorithm. In order to clarify the impact of microvibration on the interferometer under such circumstances, and to determine the critical value of microvibration that the interferometer can withstand, this paper proposes a quantitative analysis and evaluation method.

1 Homogeneity of interferometer optical range difference velocity

The velocity uniformity of an interferometer's motion mechanism can be quantitatively determined by the stability of the interferometric optical range difference velocity. In order to satisfy high-precision spectral detection tasks, interferometers need to ensure a sufficiently high stability of the optical range difference velocity, which has to be realised by the precision motion of the kinematic mechanism[5].

1.1 Interferometer optical range difference

The angular mirror translation interferometer achieves the scanning of the optical range difference by the translation of the angular mirror (cubecorner) driven by the voice coil motor and the fixation of the fixed mirror. The interferometer optical path is shown in Figure 1.

In FIG. 1, the measured collimated beam is divided into a reflected beam A on the beam splitter mirror and FIG. 1, the measured collimated beam is divided into a reflected beam A and a transmitted beam B on the beam splitter mirror, the A beam is reflected back through the angular mirror CC1 and reflected through the beam splitter mirror and reaches the detector; while the B beam is reflected back through the angular mirror CC2 and then reflected through the beam splitter mirror and reaches the detector as well. In this way, beams A and B produce interferogram signals on the detector. Definition of A, B beams of light equal position, that is, the figure CC1 and CC2 location for the interferometer zero path difference position (zero path difference, ZPD).

When the voice coil motor drives the angular mirror CC2 to move a distance L, relative to the ZPD position, the B beam travels 2 mechanical path differences L, so at this time the optical path difference (optical path difference, OPD) between beams A and B is 2L.

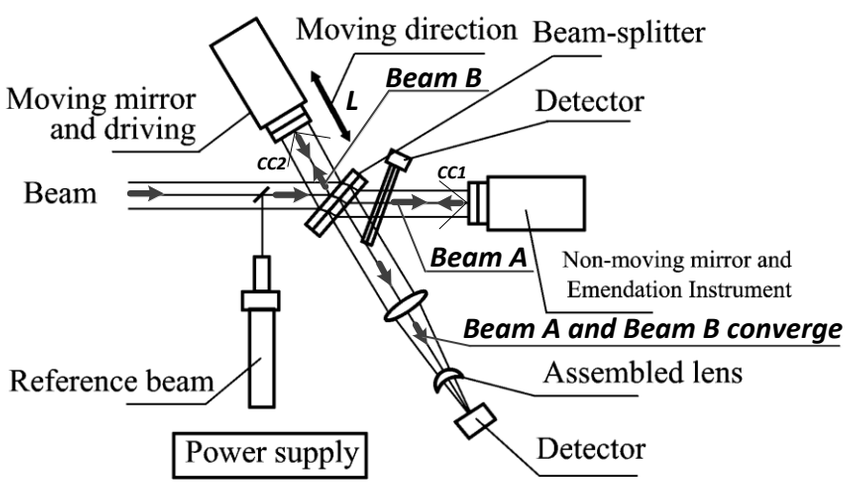

Fig. 1 Interferometer optical path difference (OPD)
图1 干涉系统光程差示意图

Thus the optical range difference *D of* the angular mirror translational interferometer is[6-7]

$$D = 2L(t) \quad (1)$$

1.2 Interfering optical range difference velocity stability

The optical range difference velocity $v = \frac{d}{dt}D(t)$, according to equation (1).

$$v = 2\frac{d}{dt}L(t) \quad (2)$$

From Eq. (2), it can be seen that the optical differential velocity depends on the velocity $\frac{d}{dt}L(t)$. Uniform scanning modulation of the interferometer optical range difference requires that the speed v of the optical range difference be uniform.

The uniformity of the optical range difference velocity is generally quantitatively described by the optical range difference velocity stability. Firstly, the instability of the optical range difference velocity is defined as α. α is the ratio of the standard deviation to the mean value of all optical range difference velocity samples taken by the interferometer angular mirror in the effective range of the optical range, and it is generally required that $\alpha < 1\%$[8-9]; the stability of the optical range difference velocity is defined as $(1-\alpha)$, and it is generally required that $(1-\alpha)$ is >99%.

2 Interferometer Optical Surface Rigid Body Motion

For analysis using finite elements, the finite element model of an optical element is defined as a shell or solid cell, and the optical surface is characterised by a number of grid nodes, with the average rigid-body motions of the surface (translational displacements T_x、T_y、T_z and rotational displacement R_x、R_y、R_z) is characterised by an area-weighted average motion [3]. For a node $i(x_i, y_i, z_i)$ its rigid-body displacements d_{xi}、d_{yi} and d_{zi} are expressed as

$$\begin{cases} d_{xi} = T_x + z_i R_y - y_i R_z \\ d_{yi} = T_y - z_i R_z + x_i R_z \\ d_{zi} = T_z + y_i R_z - x_i R_y \end{cases} \quad (3)$$

According to the principle of least squares best fit, the surface displacements obtained from the finite element analysis are post-processed using Matlab programming, then the actual optical element surface node displacements D_{xi}、D_{yi}、D_{zi} (vector-height displacement) and the nodal rigid body displacement d_{xi}、d_{yi} and d_{zi} The squared difference between the actual optical element surface node displacement (vector height displacement) and the node rigid body displacement E is

$$E = \sum_i \omega_i \left[(D_{xi} - d_{xi})^2 + (D_{yi} - d_{yi})^2 + (D_{xi} - d_{zi})^2\right] \quad (4)$$

Eq: ω_i is the weighting factor.

The best fit for the rigid body motion is obtained by substituting equation (3) into equation (4), taking partial derivatives for each term and making its derivative equal to dry zero. The resulting system of simultaneous equations for the mean rigid body motion is

$$\begin{aligned}
&\sum_i \omega_i D_{xi} = \sum_i \omega_i T_x + \sum_i \omega_i z_i R_y - \sum_i \omega_i y_i R_z \\
&\sum_i \omega_i D_{yi} = \sum_i \omega_i T_y + \sum_i \omega_i x_i R_z - \sum_i \omega_i z_i R_x \\
&\sum_i \omega_i D_{si} = \sum_i \omega_i T_z + \sum_i \omega_i y_i R_x - \sum_i \omega_i x_i R_y \\
&\sum_i \omega_i (z_i D_{yi} - y_i D_{si}) = \sum_i \omega_i z_i (T_y + x_i R_z) - \\
&\quad \sum_i \omega_i y_i (T_z - x_i R_y) - \sum_i \omega_i R_x (z_i^2 + y_i^2) \\
&\sum_i \omega_i (z_i D_{xi} - x_i D_{si}) = \sum_i \omega_i z_i (T_x - y_i R_z) - \\
&\quad \sum_i \omega_i x_i (T_z + y_i R_x) + \sum_i \omega_i R_y (z_i^2 + x_i^2) \\
&\sum_i \omega_i (y_i D_{xi} - x_i D_{yi}) = \sum_i \omega_i y_i (T_x + z_i R_y) - \\
&\quad \sum_i \omega_i x_i (T_y + z_i R_x) - \sum_i \omega_i R_z (y_i^2 + x_i^2)
\end{aligned} \quad (5)$$

The optical model of the angular mirror translational interferometer is shown in Fig. 2. An uptake is applied to the moving mirror fixed mirror and beam splitter along the three axes and in the direction of rotation around each axis to obtain the sensitivity coefficients of the system's optic-axis error, each of which is the offset of the image divided by the input value of the uptake. For this optoelectronic system, ignoring the terms with small sensitivity coefficients, the equation of motion of the image in the focal plane can be derived as

$$\begin{aligned}
\Delta_x &= \varphi_{M1,T_x} T_{M1,x} + \varphi_{M1,R_y} R_{M1,y} + \varphi_{M2,T_x} T_{M2,x} + \\
&\quad \varphi_{M2,R_y} R_{M2,y} + \varphi_{IP,T_x} T_{IP,x} \\
\Delta_y &= \varphi_{M1,T_y} T_{M1,y} + \varphi_{M1,R_x} R_{M1,x} + \varphi_{M2,T_y} T_{M2,y} + \\
&\quad \varphi_{M2,R_x} R_{M2,x} + \varphi_{HP,T_y} T_{HP,y}
\end{aligned} \quad (6)$$

Eq: φ is the sensitivity coefficient; T、R denote the translational and rotational displacements, respectively; the subscripts M1, M2, and IP correspond to the moving mirror fixed mirror and beam splitter, respectively; Δ_x and Δ_y are the image motion in x and y direction of the image motion, respectively.

3 Methods of analysing the effects of microvibration

The work in this paper is aimed at identifying the critical value of microvibration that the interferometer can withstand when the mechanism control system's guarantee of the uniformity of the speed of the moving mirror's linear motion is not clear. Since the influence of the

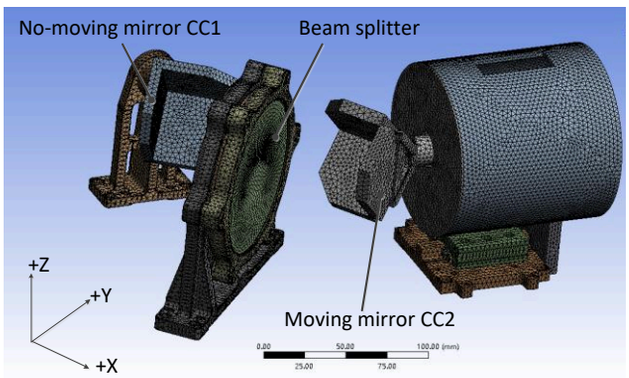

Fig. 2 Finite element model of the interferometer
图2 干涉系统有限元模型示意图

control system is not clear, the analysis process assumes that it has no influence on the external environment. It is assumed that the linear travel of the moving mirror at any transient moment under microvibration is a linear superposition of the pendulum angle of this control system and the pendulum angle due to microvibration. Such a linear travel of the moving mirror of the interferometer is then used to derive results on the homogeneity of the differential velocity of the optical path, and to quantify the effect of the microvibration on the reliability of the interferometer under a given mechanism control system.

This method of analysis incorporates the microvibration-induced interferometer response into the analysis of the mechanism's kinematic stability, which ensures more realistic reliability analysis results.

3.1 Underlying assumptions

Microvibration excitation directly affects interferometer travel $D(t)$ and motion velocity $\frac{d}{dt}\mathrm{D(t)}$. It is assumed that under microvibration conditions, the motion travel $D(t)$ is the motion stroke controlled by the mechanism control system $D_c(t)$ and the motion travel caused by microvibration $D_d(t)$ The linear superposition of, i. e.

$$D(t) = D_c(t) + D_d(t) \tag{7}$$

It should be noted that here the movement stroke of the mechanism control system $D_c(t)$ does not include velocity uniformity then interferometer velocity uniformity is guaranteed.

Then the speed of motion of the moving mirror of the interferometer

$$\frac{d}{d_t}D(t) = 2\frac{d}{d_t}L_c(t) + 2\frac{d}{d_t}L_d(t) \tag{8}$$

At this point the optical range difference of the interferometer is

$$\mathrm{D} = 2L_c(t) + 2L_d(t) \tag{9}$$

It can be seen that the differential optical velocity under the influence of microvibration is a function of 2 variables.

3.2 Kinematic properties of translational angular mirrors

With the above mechanism control system, the interferometer moving mirror movement distance $D_c(t)$ and speed $\frac{d}{dt}D_c(t)$ are derived. According to equation (2) there are

$$\mathrm{v \cdot t = L(t) + c} \tag{10}$$

Where c is a constant. Definition $t = 0$, the interferometer angular mirror is located in the optical zero position (ZPD), at this time the interferometer angular mirror movement time $t = 0$, so $c = 0$. Therefore, the stroke of the interferometer angular mirror under the mechanism control system is $\mathrm{L(t)}$ Therefore, the travel of the interferometer mirror under the mechanism control system is

$$\mathrm{v \cdot t = L(t)} \tag{11}$$

The microvibration-induced velocity response v and velocity response d (v) of the interferometer's moving mirror angular mirror travel can be obtained by discrete time-domain response solving with a finite element model of the interferometer structure.

4 Analysis of microvibration effects in angular mirror translational interferometers

The angular mirror translational interferometer, shown in figure 2, is connected to the satellite platform by means of mounting lugs. The platform is equipped with a flywheel and carries multiple scanning mechanisms and chiller loads. The platform vibration excitation frequencies are concentrated at 90 Hz, 70 Hz, 50 Hz and 30 Hz, and the micro-vibration is excited in the three main-axis directions simultaneously on the interferometer mounting lugs. In order to clarify the effect of the platform perturbations on the operation of the interferometer, the velocity uniformity of the interferometer under the above excitations is analysed using the method described in this paper.

The interferometer has two modes of operation and the associated parameters are shown in Table 1.

Firstly, the travelling distance and speed of the motion under a certain mechanism control system are solved. According to the Rayleigh criterion, the spectral

Tab.1 Parameters of the interferometer
表1 某型干涉系统参数

Interferometer characteristic terms	Working mode
Maximum optical range difference during motion Dmax /mm	5
Required differential optical velocity v / (mm/s)	0.2
Spectral Resolution $\Delta_{M\sigma}$ (cm^{-1})	0.5

resolution limit is $1/2\Delta_M$ which is determined by the maximum optical range difference generated by the moving mirror movement. Therefore, the larger the optical range difference, the higher the spectral resolution of the instrument.

Then using the interferometer structure finite element model (Figure 3), the time domain response is solved to obtain the response of the pendulum arm angle and angular velocity caused by microvibration. According to the frequency characteristics of the platform disturbance source, the microvibration conditions are selected as 12 working conditions with frequencies of 90Hz, 70Hz, 50Hz, 30Hz, and acceleration amplitudes of $50\times10^{-3}g_n$, $30\times10^{-3}g_n$, and $10\times10^{-3}g_n$ combinations, and the simultaneous excitation of three spindle directions is considered.

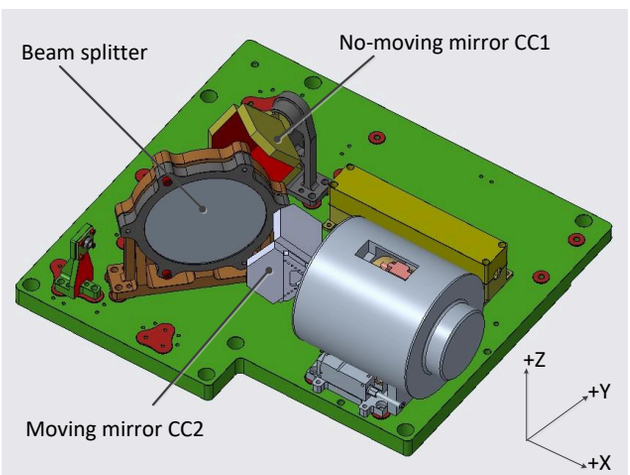

Fig. 3 Model of the interferometer
图3 干涉系统结构示意图

Thus, the mean value of the optical range difference velocity is $E=\frac{\sum_{i=1}^{N}v(t_i)}{N}$ The standard deviation of the optical differential velocity is $\sigma=\sqrt{\frac{\sum_{i=1}^{N}[v(t_i)-E]^2}{N}}$ The stability of the optical differential velocity under the above microvibration conditions is shown in Table 2.

Table 2 Optical range difference velocity stability under microvibration conditions
表2 振颤工况下光程差速度稳定性

Microvibration frequency / Hz	Optical range difference velocity stability/%		
	$50\times10^{-3}g_n$	$30\times10^{-3}g_n$	$10\times10^{-3}g_n$
90	98.54	98.4	99.3
70	98.6	98.76	99.39
50	98.86	99.32	99.57
30	99.34	99.48	99.81

Finally, the obtained control system and the results of the microvibration-induced angle-mirror travel analysis are substituted into Eq. (2) to obtain the time-domain values of the optical differential velocities of the interferometer angle-mirror motion under microvibration conditions $v(t_i)$, i = 1, 2, 3, ..., N, where N is the total number of moments in the finite element time domain discretisation. The time-domain transient process of the interferometer mirror travelling is obtained by solving the time-domain curve as in Fig. 4. This overview can be approximated as a linear function and is represented as a target velocity value in figure 4.

The time-domain curve contains information about the value of the mirror travelling caused by the whole time-domain process of the microvibration action. Fig. 5 is the schematic diagram of the mechanical experiment. The transient process of the velocity motion of the moving mirror is shown in Fig. 4 under the conditions of 50×10^{-3} g_n, 30×10^{-3} g_n and 10×10^{-3}gn with frequencies of 90Hz.

Analysing Table 2 the following conclusions can be obtained, under a certain control system:

1) The smaller the magnitude of the vibration acceleration, the higher the stability for a given microvibration frequency.

(2) For a certain magnitude of microvibration acceleration, the lower the vibration frequency, the higher the stability.

(3) Overall, when the microvibration amplitude magnitude is in the order of 10×10 - 3gn, the interferometer optical range difference velocity stability ($1-\alpha$) at all frequencies meets the basic requirement of >99%.

Desktop micro-vibration tests were carried out on the flat-acting angular mirror mechanism, and the test results are shown below. A comparison of the test programmes is shown in Fig. 5.

As shown in Table 2, at the same amplitude, the velocity uniformity becomes worse as the frequency increases, so the Fourier transform calculation is performed at 90 Hz when the velocity uniformity is greater than 99% and the vibration conditions are the worst. The result, shown in Figure 6, meets the design criteria.

5 Conclusions

To address the problem of the interference of in-orbit microvibration on the precision motion of spectral detection interferometer mechanisms, a more comprehensive method of analysing the interferometer optical range difference velocity uniformity is proposed. The method incorporates the microvibration-induced structural response of the interferometer as an influencing factor into the analysis of interferometer stability, which can reflect the reliability of the interferometer on-orbit working state more realistically than the usual method of equating the influence of external excitation to a certain influencing factor[10-14]. This method allows to quickly determine the critical values of the interferometer's microvibration magnitude in conditions where the organisation's control algorithms for external environmental excitations are not well defined. Considering that the control algorithm is usually an improvement of the external environment, this critical value has a certain safety margin. Therefore, this method

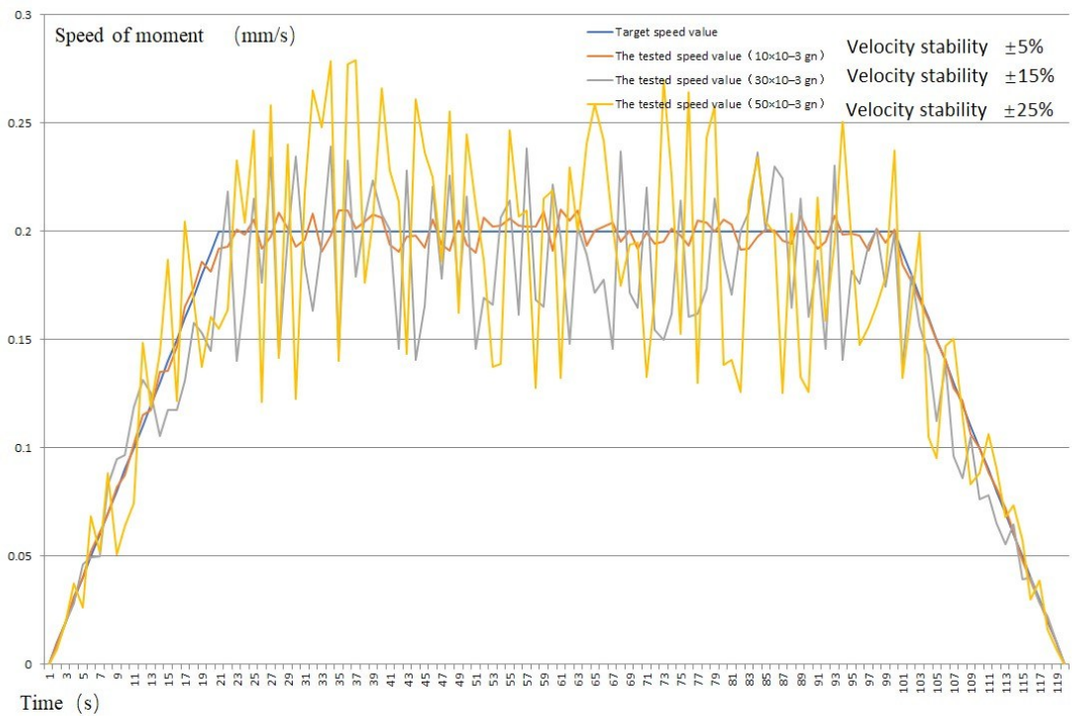

Fig. 4 Analysis results in discrete time sequence
图4 干涉系统速度在不同时刻分析结果

has some application value in solving practical engineering problems.

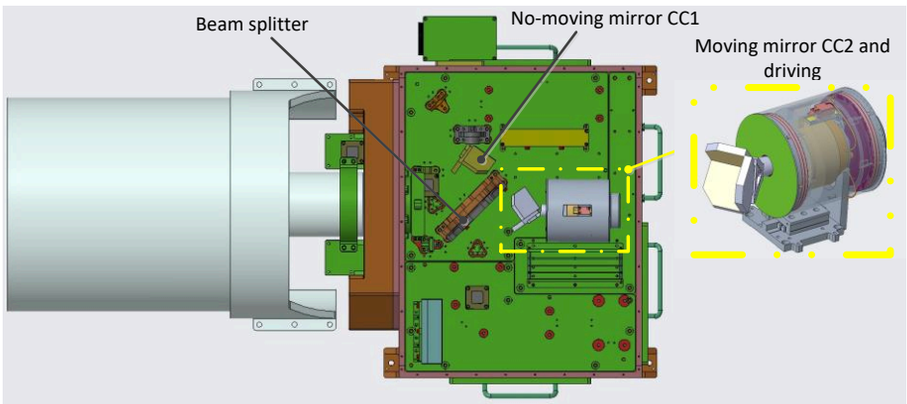

(a)

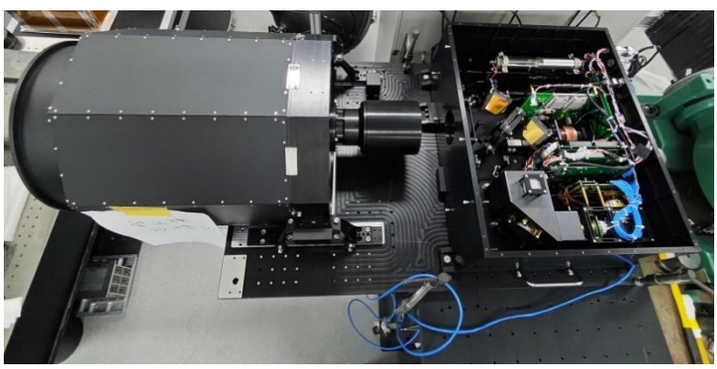

(b)

Fig. 5 Instrument structure of the interferometer based on the angular mittor translation system
图5 基于角镜平动式干涉系统的仪器结构图

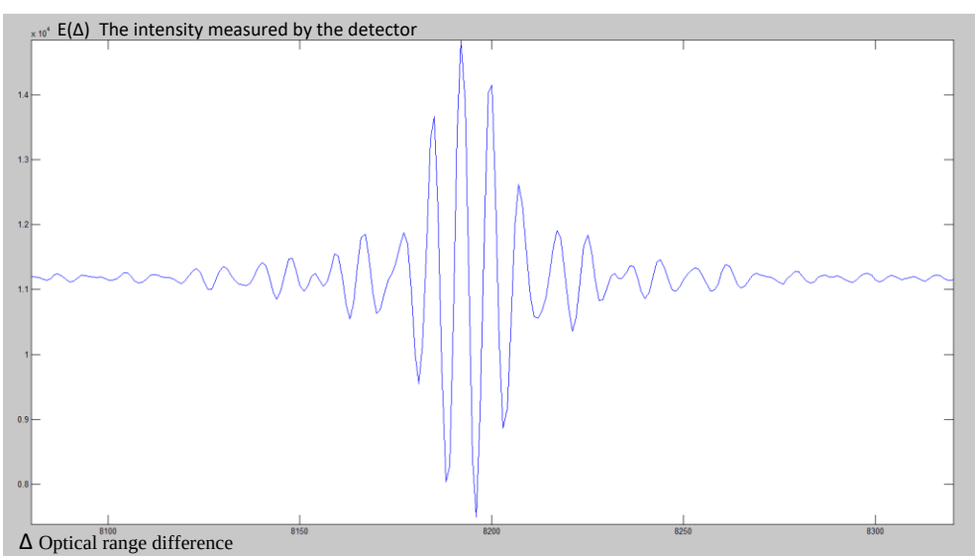

Fig. 6 Plot of test results of the planar angular mirror mechanism programme
图6 基于角镜平动式干涉系统的测试结果图

References

[1]XING Ting, GONG Huixing. Space Borne Fourier Transform Spectrometer for Atmospheric Sounding[J]. Remote Sensing Technology and Application, 1999, 14(1): 5-10.
[2]Marc-Andre Soucy, Francois Chateauneuf, Christophe Deutsch, et al. ACE-FTS Instrument Detailed Design [J]. Proceedings of the SPIE, 2002, 4814: 176-188.
[3]Nassar R, Boone C, Walker K A, et al. Sci Sat-1: Retrieval Algo-

rithms, ACEFTS Testing and the ACE Database[J]. Proceed-ings of SPIE, 2004, 5151: 173-183.
[4] Jacques Giroux, Louis Moreau, Guillaume Girard, et al. Technological Evolutions on the FTS Instrument for Follow-on Mission to SCISAT Atmospheric Chemistry Experiment[J]. Proceedings of SPIE, 2010, 7826: 7826-1A.
[5] Hiroshi Suto, Akihiko Kuze, Kei Shiomi, et al. On Orbit Status of TANSO-FTS on GOAST[J]. Proceedings of SPIE, 2010, 7826: 7826-04.
[6] Brad Gom, David Naylor. Testing Results and Current Status of FTS-2, an Imaging Fourier Transform Spectrometer for SCUBA-2[J]. Proceedings of SPIE, 2010, 7741: 77412E-1.
[7] Francois Chateauneuf, Serge Fortin, Chantal Frigon, et al. ACE-FTS Test Results and Performance[J]. Proceedings of SPIE, 2002, 4814: 82-90.
[8] Comolli L, Saggina B. Analysis of Disturbances in the Planetary Fourier Spectrometer Through Numerical Modeling [J]. Planetary and Space Science, 2010, 58:864-874.
[9] XU Jiarong. On the High Optical Spectrum Interference Imaging Spectrometer[D]. Nanjing: Nanjing University of Technology, 2008.
[10] Jyrki Kauppinen, Pekka Saarinen. Line-shape Distortions in Misaligned Cube Corner Interferometers[J]. Applied Optics, 1992, 31(1): 69:74.
(Tokuno M. Improvements in the method to extract operational cloud motion winds and water vapor motion winds of the GMS-5 system [EB/OL]. [2022-03-06]. http://cimss. ssec. wisc. edu/iwwg/iww4/p61-68_Tokuno-Improvements.pdf.
[11] Holmlund K, Grandell J, Schmetz J, et al. Meteosat third generation (MTG): continuation and innovation of observations from geostationary orbit [J]. Bulletin of the American Meteorological Society, 2021, 102(5): E990-E1015.
[12] Ma Z, Li J, Han W, et al. Four-dimensional wind fields from geostationary hyperspectral infrared sounder radiance measurements with high temporal resolution[J].Geophysical Research Letters, 2021, 48(14): 093794.
[13] Stevens M H, Englert C R, Harlander J M, et al. Retrieval of lower thermospheric temperatures from O_2A band emission: the MIGHTI experiment on ICON[J]. Space Science Reviews, 2018, 214(1): 4.
[14] Xu G Q, Zhang Y F, Wan J W, et al. Application of high-resolution three-dimensional imaging lidar[J]. Acta Optica Sinica, 2021, 41(16): 1628002.